WJCMS

Wasit Journal of Computer and Mathematics Science

Journal Homepage: https://wjcm.uowasit.edu.iq/index.php/WJCM

e-ISSN: 2788-5879 p-ISSN: 2788-5879

Ant Colony Optimization (ACO) Based Fuzzy C-Means (FCM) Clustering Approach for MRI Images Segmentation

Mohammed H. Al Aqad[1,*] and Luis Miguel Oliveira de Barros Cardoso[2]

[1]Department of Social Sciences at Management and Science University, Malaysia

[2]Department of Languages and Communication Sciences, Polytechnic Institute of Portalegre, Portugal

*Corresponding Author: Mohammed H. Al Aqad

DOI: https://doi.org/10.31185/wjcms.230

Received: August 2023; Accepted: November 2023; Available online: December 2023

ABSTRACT: Thousands of real-life ants have been used to improve the Ant Colony Optimization (ACO) technique. Significant improvement can be noticed in segmented images using ACO-based rather than random initialization. The segmentation quality has improved as a result of the noise reduction. Clustering based on FCM is used to segment medical images. To avoid local optimal results, cluster centres are initially determined using ACO. This paper shows that our approach (ACO-FCM) provides significant improvements. In ACO-FCM, brain tissues are classified more accurately because there are more correctly classified pixels. As a result of our approach, such tissues can be classified more accurately based on spatial information.

Keywords: Ant Colony Optimization, Clustering, MRI, Images Segmentation

CC BY

1. INTRODUCTION

Different image processing techniques rely on image segmentation. Images may be segmented according to certain properties or characteristics to make viewing easier. The intensity, texture, colour, and so forth of every pixel in a region are similar. Segmentation facilitates analysis and visualization by removing irrelevant information. In addition to medical imaging and face recognition, segmentation has spread to domains like automatic traffic control systems, machine vision, expert systems, and satellite imagery. As a result of its various practical applications, medical image segmentation has become a hot topic. Anatomical segments can be separated from the brain (e.g., to extract brain tumours or certain main tissues, such as W.M., G.M., CSF) or the brain can be segmented according to its arrangement [1–4] in medical images, there are various artefacts such as noise, bias fields and partial volume effects which create a higher degree of complexity than in other images [5, 6].

Grey matter, white matter, and cerebrospinal fluid are the three tissue categories that can be classified from brain MRI images. When decoding images, random noise, bias fields, and partial volume effects can be tedious and challenging. Medical Images are segmented using a modified Fuzzy C-means clustering method [7, 8]. To avoid local optimal results, cluster centres are initially determined using ACO. Since data points aren't always distributed spherically, Mahalanobis distance is used instead. Typically, medical images contain random noise, so this Algorithm is used to segment them. The clustering process also considers spatial information, such as local neighbourhood information. Due to noise, the film is ineffective compared to the results.

2. LITERATURE REVIEW

Using Ant Colony Optimization (ACO), real-life scenarios influence how ants behave. Problems classified as NP-hard are solved with it [9]. ACO is the probabilistic approach that solves discrete optimization based on difficult problems [10]. Numerous real-life applications have utilized different image segmentation techniques [11]. We are most concerned about soft clustering, which involves objects belonging to various clusters/classes with varying degrees of membership. Fuzzy C-means algorithms are commonly used in soft clustering [12, 13]. This approach simplifies the implementation of clustering while ensuring efficiency. However, when there is noise, FCM does not deliver the results expected. In addition to considering random values in the initialization step, the entire Algorithm does not consider spatial information. Spatial data and information have been incorporated into several works [14, 15]. [16] developed FCM-S in which grey levels were included in the objective function; however, this technique was computationally expensive [14]. For each data point, we propose a variant of FCM that computes the neighbouring terms ahead of time. Data points are also distanced from cluster centres using Euclidean measures in FCM. As a result of Euclidean distance, spherical data points from a point are always considered. Correlations between data points are not taken into account. In addition to distance, direction determines whether a data point belongs to the same cluster. Both of these issues were considered by P.C. Mahalanobis in 1936 when he introduced the Mahalanobis distance [17]. According to the evidence presented, Mahalanobis distance is not directly applied to clustering. The authors [18] introduced a fuzzy covariance matrix using Mahalanobis distance with fuzzy terminology in this work. We additionally introduce meta-heuristic approaches for problems with uncertain or not readily available data, such as NP-hard problems. Particle swarm optimization, genetic algorithms, and ant colonies are also optimization methods. Author [19] FCM-compatible extension of simplified ant colony system. Authors [20] presented ACOA in which ants were moved randomly from one solution set to another using array-based graphs.

3. METHODOLOGY

An automated segmentation framework is presented in this paper for white matter, grey matter, and cerebrospinal fluid. These tissues are segmented using MRI images of the brain. It is often the initialization step that determines the results of segmentation. Noise is often present in MRI images. An important segmentation algorithm is FCM. An Ant Colony Optimization technique prevents getting stuck in local optimal results. The ACO determines an initial cluster centre's value. Segmentation is performed using the centres thus obtained. W.M., G.M., and CSF are segmented using modified Fuzzy C-means clustering. As Euclidean distance ignores shapes other than super spherical, Mahalanobis distance is instead used in modified FCM to cluster data opinions. Data facts may belong to a similar cluster located outside of that area. In addition to pixel information about neighbouring pixels, local neighbourhood information is also considered as pixels tend to belong to the same cluster.

3.1 INITIALIZATION STEP USING ANT COLONY OPTIMIZATION

ACO describes how ants behave in the real world and is based on probabilistic optimization principles. To find the shortest route between a pheromone source and a destination/food source, several optimization problems can be simplified based on the pheromone concentration. As FCM is highly noise-sensitive, Fuzzy C-means clustering algorithms [19] can easily become trapped in local optimal solutions. To get the best solution, each time one runs the Algorithm with different initial values, comparing the results with the best result each time [21]. It is, however, a very time-consuming process. Incomplete data can be solved using meta-heuristic optimization techniques. (B Meta-heuristic optimization techniques can solve incomplete, noisy, or uncertain data. You can find the global optimal solution with Ant Colony Optimization without slipping into local optimality. As a solution to the problem of segmenting brain tissues, Ant Colony Optimization is proposed. Brain MRI images are segmented using ACO to determine initial cluster values.

Table 1. Parameters values used in ACO initialization

Parameters	Values
$\alpha = \beta$	1.6
total_Number of Ants	10
Max_iteration	160
Rho (ρ)	0.2

3.1.1. Algorithm for initialization using ACO (ACO-FCM)

Requirements: All parameters in Table 1 should be initialized, including the number of clusters.

Step1: Here is an input data matrix/image $X = (X_1, X_2, \ldots\ldots X_n\}$, with a pixel count of n.

Step 2: Compute every pixel's mean value in a second matrix, X', whose dimensions are the same as X.
Step3: Iterate up to max_iteration for iter =1
Step4: For ants=1, do the following
Step5: All clusters 'c' should be randomly initialized with cluster centre values
Step6: Using $\eta = \frac{1}{D}$As a heuristic matrix, calculate a heuristic matrix η based on each pixel's distance from each cluster centre.
Step7: Using the formula, calculate the probability that each pixel is associated with a particular cluster

$$P_{ij} = \frac{\left(\tau_{ij}^{\alpha}\right)\left(\eta_{ij}^{\beta}\right)}{\left(\sum_{\Omega\in \text{ sllowed}}\left(\tau_{ij}^{\alpha}\right)\left(\eta_{ij}^{\beta}\right)\right)} \tag{1}$$

Step8: The cluster centres of each pixel are updated using the following formula after each pixel is indexed into different clusters calculated via the above probability:

$$V_j = \left\{\frac{\sum_{i\subseteq S}\left(u_{i,j}\right)^m x_i + \alpha * x_i^{'})}{\sum_{i\subseteq S}(1+\alpha)*\left(u_{i,j}\right)^m}\right\}, \quad \forall_j = 1, 2 \ldots\ldots n_c \tag{2}$$

A cluster number S is a group of pixels with a similar index, i.e., similar cluster numbers.
Step 9: Apply the updated cluster centres to the Euclidean distance calculation.
Step10: Using the calculated distance above, calculate the objective function as follows:

$$J = \sum_{i=1}^{n}\sum_{j=1}^{c}\left(u_{i,j}\right)^m d^2(x_i, C_j) + \alpha\sum_{i=1}^{n}\sum_{j=1}^{c}\left(u_{i,j}\right)^m d^2(x_i^{'}, C_j) \tag{3}$$

Step 11: Assess the best fitness concerning objective function. The fitness function should be minimized. Every pixel in an image is updated with the best fitness, best centres, and corresponding indexes.
Step11: This is the end of the loop (at step 4)
Step12: Utilize the best centres to calculate the distance after each iteration
Step13: Using the updated distance, update the membership matrix

$$U_{i,j} = \frac{\left(d^2\left(x_i, C_j\right) + \propto d^2\left(x_i^{'}, C_j\right)\right)^{\frac{1}{(m-1)}}}{\sum_{k=1}^{nc}\left(d^2\left(x_i, C_j\right) + \propto d^2\left(x_i^{'}, C_j\right)\right)^{\frac{1}{(m-1)}}} \tag{4}$$

Step14: For each pixel, determine the best index by using the best solution following each iteration
Step15: Utilize the best indexes from the previous step to update the pheromone matrix:

$$\tau_{i,j} = (1-\rho) * \tau_{i,j} + \Delta\tau_{i,j} \tag{5}$$

$\Delta\tau_{i,j} = \frac{1}{distance}$ pheromone update is being conducted at the same location
Step16: This is the end of the loop for step 3 of the max_iteration loop
Step 17: Return the membership matrix associated with the best centres obtained.
FCM does not affect segmentation results because it is run on a noisy image. This results in a degraded segmentation quality, as no noise reduction can be seen in the resultant image. Significant improvement can be noticed in segmented images using ACO-based rather than random initialization. The segmentation quality has improved due to the noise reduction.

4. RESULT ANALYSIS AND DISCUSSION

MRI images taken from Insight Journal have been analyzed in real time. A medical image processing and visualization domain is covered by the Insight Journal, which is an open-access online publication. In addition to MIDAS, it publishes other journals as well. NAMIC, a community of Midas users presents data from two autistics and two non-autistics (male and female). After two years, the data are recollected. There are 3 types of MRI skimming accessible, namely images with T_1 weights, images with T_2 weights, and images with T_2 weights. A slice thickness of 1.5mm is used to obtain coronal slices. With the database, you will also find a map of tissue segmentation labelling. Atlas-based tissue segmentation is used in this tissue label by taking advantage of expectation-maximization techniques. Based on the ground truth images,

Table 2. **Classification of Pixels for ACO-FCM**

Patient #	Ground_True	True_positive	False_negative	False_Positive
Autistic Female slice100	34482	29779	4703	2172
Autistic Female slice140	33936	29829	4017	4449
Control Female slice80	33056	30733	2323	3581
Control Female slice114	28503	24764	3739	3946
Control Male slice110	33528	28973	4555	5197
Control Male slice67	39125	34822	4303	4442
Autistic Male slice70	30248	28660	1588	3036
Autistic Male slice160	10960	10183	777	809

quantitative analysis is conducted on MRI brain images (Table 2). Pixels that are classified correctly are called true positives. True negative counts pixels that do not appear in ground truth but are classified by our system as belonging to a cluster, while False positive counts pixels that do not appear in ground truth but are classified by our system.

The accuracy of segmentation can be measured quantitatively using several schemes [22, 23]. Here are a few of them:

5. DICE COEFFICIENT

$$D(P,Q) = \frac{2\,|P \text{ and } Q|}{|P+Q|} \tag{6}$$

6. SET CONTAINS P, AND A SET CONTAINS Q, WITH | | REPRESENTING THEIR SIZE

There is a range of 0 to 1 for the dice coefficient. There is no match/overlap if the value is 0, and if the value is 1, there is a complete match/overlap. Segmented images are represented by P, while ground truth images are represented by Q.

7. JACCARD'S COEFFICIENT

$$J(P,Q) = \frac{P \text{ intersection } Q}{P \text{ union } Q} \tag{7}$$

It is also between 0 and 1 if the Jaccard similarity is considered. In the case of a match/overlap, 0 indicates no match, and 1 indicates an exact match/overlap. Jaccard similarity and Dice constant have the following relationship:

$$D + 2 * \frac{J}{(1+J)} \tag{8}$$

8. TRUE POSITIVE FRACTION (SENSITIVITY)

$$TPF = \frac{TP}{TP+FN} \tag{9}$$

True Positives - TP, False Negatives - FN.

9. FUZZY PARTITION COEFFICIENT (F_{PC} AND FUZZY) PARTITION ENTROPY (F_{PE})

The cluster validity functions can be used to evaluate clustering algorithms quantitatively. The best clustering results are obtained when partition coefficients and entropies are minimized. In addition to considering the fuzzy partition, these two parameters don't take into account specific features.

$$f_{PC}(U) = \frac{1}{N} * \sum_{p=1}^{N} \sum_{q=1}^{nc} u_{p,q}^{2} \tag{10}$$

$$f_{PE}(U) = -\frac{1}{N} * \sum_{p=1}^{N} \sum_{q=1}^{nc} u_{p,q}^{2} * log(u_{p,q)} \tag{11}$$

Table 3. The Dice Coefficients are calculated using our approach (ACO-FCM) and standard FCM.

Dice Coefficient									
ACO-FCM					FCM				
Patient #	G.M.	WM	CSF	Avg.	Patient #	G.M.	WM	CSF	Avg.
P-11	92.8	88.9	75.5	85.7	P-11	91.7	84.8	57	77.8
P-12	86	92.7	78.5	85.7	P-21	83.8	84.8	68	78.8
P-21	90.2	93.3	87.8	90.4	P-21	84.9	83	78.4	82.1
P-22	89.9	80.6	75.9	82.1	P-22	87.2	75.1	61.7	74.6
P-31	88.7	80.2	79.6	82.8	P-31	84.1	79.3	65.2	76.2
P-32	90.3	88.8	79.8	86.3	P-32	85.2	81.7	71.6	79.5
P-41	92.4	94	85.9	90.7	P-41	88.7	84.6	83.8	85.7
P-42	95.4	81.4	85.3	87.3	P-42	91.8	74.4	69.7	78.6
Average	90.7	87.4	81	86.3	Average	87.1	80.9	69.4	79.1

The dice coefficient measures volume overlap based on segmentation capacity pairs. NIMAC provides several slices of male and female datasets showing normal and autistic individuals. A Dice Coefficient average was calculated from several runs. In comparison with standard FCM, we observe that our approach (ACO-FCM) provides significant improvements. Brain tissue classification is more promising in ACO-FCM because more pixels are correctly classified. As a result of our approach, such tissues can be classified more accurately based on spatial information. It is better to have a dice coefficient close to 1 if segmentation accuracy is important. Generally, dice coefficients greater than 0>7 indicate good segmentation. Jaccard's similarity measure is similar to the Dice Coefficient. Overestimations and underestimations of volume do not affect either of these parameters. There is, however, a stronger correlation between the dice coefficient and Jaccard ratio when volumetric overlaps are strong, resulting in mismatches. A better understanding of the classification system can be gained by examining the estimated results using Jaccard's ratio.

$$J = \frac{D}{2 - D} \tag{12}$$

J- Jaccard's ratio, D- Dice coefficient

Cerebrospinal fluid classification affects the accuracy of classification/segmentation. Similarly, grey matter and white matter tissue segmentation accuracy has improved, but the CSF segmentation accuracy has changed significantly. Our brain's CSF (fluid) is an extremely complex tissue. In brain MRIs, a flowing matter is occasionally difficult to segment. Thus, it is imperative to categorize CSF data points more accurately. When compared to a standard FCM approach, our approach shows an improvement. Also, we used simulated 3D images with varying noise levels to validate the ACO-FCM method for segmenting brain MRI images. Various simulated datasets are available from McGill University's Brain Website with different file extensions [24]. A size of 181x217 represents each image's size, representing normal anatomical brain structures. An evaluation of the validity of the Algorithm was performed on slices of 1mm thickness that have been T1-weighted with noise levels of 3% and 5%.

The performance of ACO-FCM at both noise levels is superior to standard FCM. FCM becomes less efficient as noise levels increase. The corrupted slice can be seen in the image below. High noise levels reduce FCM accuracy, while high noise levels enhance ACO-FCM performance.

Table 4. **Based on our approach (ACO-FCM) and standard FCM, the value of Jaccard's overlap ratio for three brain tissues is presented.**

Jaccard's Similarity									
ACO-FCM					FCM				
Patient #	G.M.	WM	CSF	Avg.	Patient #	G.M.	WM	CSF	Avg.
P-11	86.5	80	60.6	75.7	P-11	84.6	73.6	39.8	66
P-12	75.4	86.3	64.6	75.4	P-21	72.1	73.6	51.5	65.7
P-21	82.1	87.4	78.2	82.5	P-21	73.7	70.9	64.4	69.6
P-22	81.6	67.5	61.1	70	P-22	77.3	60.1	44.6	60.6
P-31	79.6	66.9	61.1	69.2	P-31	72.5	65.7	48.3	62.1
P-32	82.3	79.8	66.3	76.1	P-32	74.2	69	55.7	66.3
P-41	85.8	88.6	75.2	83.2	P-41	79.6	73.3	72.1	75
P-42	91.2	68.6	74.3	78	P-42	84.8	59.2	53.4	65.8
Average	83	78.1	67.6	76.2	Average	77.3	68.1	53.7	66.3

Table 5. **ACO-FCM and standard FCM are used to calculate Sensitivity (True positive fraction) for Gray matter, White matter, and CSF.**

Sensitivity									
ACO-FCM					FCM				
Patient #	G.M.	WM	CSF	Avg.	Patient #	G.M.	WM	CSF	Avg.
P-11	87.9	90.7	68.6	82.4	P-11	86.9	86.6	51.8	75.1
P-12	86.2	98	70.1	84.7	P-21	84.5	89.6	61.5	78.5
P-21	91.1	98.1	81	90	P-21	85.7	87.3	72.4	81.8
P-22	87.3	94	65	82.1	P-22	84.7	87.6	52.9	75
P-31	87.4	92.3	67.8	82.5	P-31	83.1	86.2	55.5	74.9
P-32	86.8	98.1	70.2	85	P-32	82	92.1	62.9	79
P-41	95.1	98.4	75.7	89.7	P-41	91.3	88.5	72.9	84.2
P-42	94	92	79	88.3	P-42	90.4	84	64.6	79.6
Average	89.4	95.2	72.1	85.5	Average	86	87.7	61.8	78.5

Table 6. **Based on our ACO-FCM approach and standard FCM, this table presents the Dice Coefficients of Gray Matter, White Matter, and CSF.**

Dice Coefficient											
ACO-FCM						FCM					
Slice#	Noise	G.M.	WM	CSF	Avg.	Slice#	Noise	G.M.	WM	CSF	Avg.
70	3%	97.2	92.1	82.2	90.5	70	3%	95.7	85.5	68.5	83.2
98	3%	93.9	97.3	90	93.7	98	3%	88.9	94.3	83.2	88.8
110	3%	91	98	84.7	91.2	110	3%	89	95.8	80.3	88.3
AVG.		94	95.8	85.6	91.8	AVG.		91.2	91.8	77.3	86.7
109	5%	92.5	97.7	88.1	91.7	109	5%	91	96.5	82.8	90.1
136	5%	94.4	91.2	88.4	91.3	136	5%	90.6	85.1	85.9	87.2
110	5%	91.2	97.2	84.5	90.9	110	5%	88.6	95.8	77.4	87.2
AVG.		92.7	95.3	86	91.3	AVG.		90	92.4	82	88.1

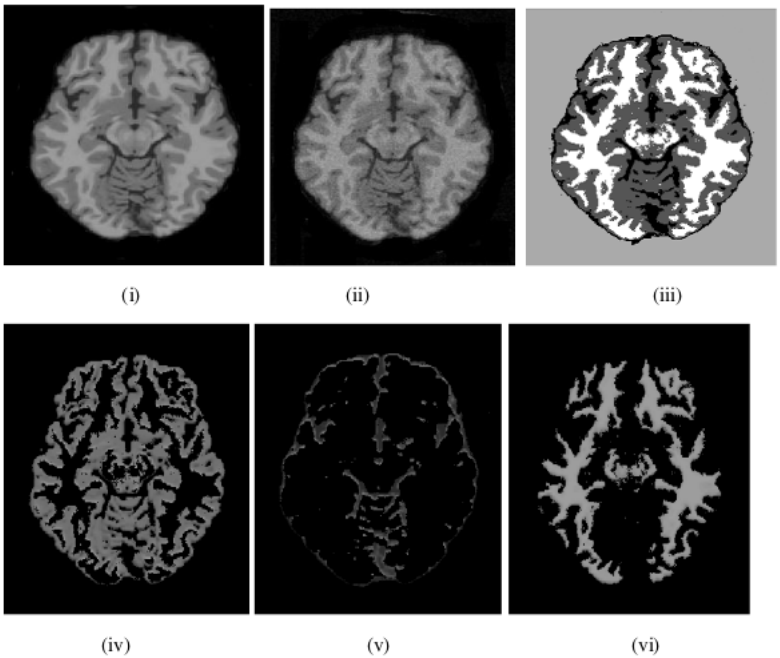

FIGURE 1. **(i) MRI T1-60, (ii) MRI with 3% noise, (iii) MRI segmented using ACO-FCM, (iv) MRI with Gray, (v) CSF, (vi) MRI with White**

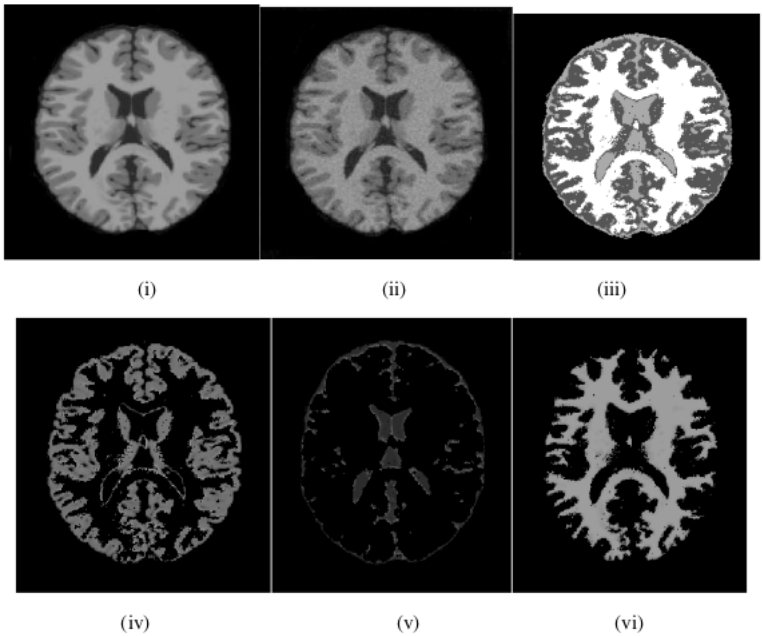

FIGURE 2. (i) MRI T1-88, (ii) MRI with 3% noise, (iii) MRI segmented using ACO-FCM, (iv) MRI with Gray, (v) CSF, (vi) MRI with White

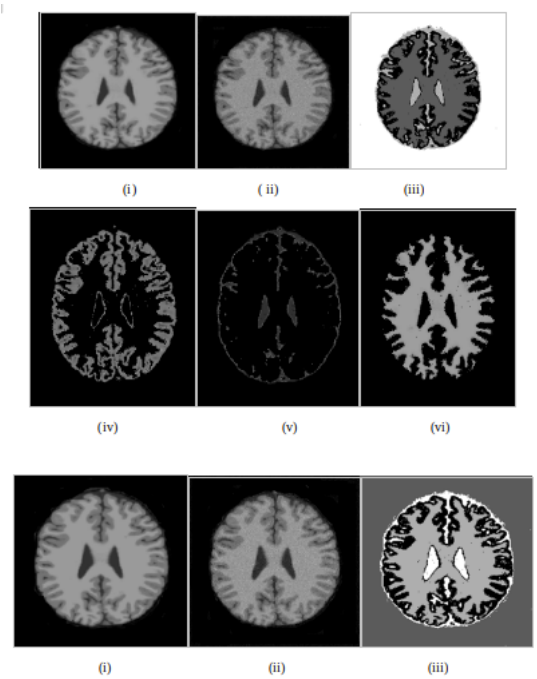

FIGURE 3. (i) MRI T1-100, (ii) MRI with 3% noise, (iii) MRI segmented using ACO-FCM, (iv) MRI with Gray, (v) CSF, (vi) MRI with White

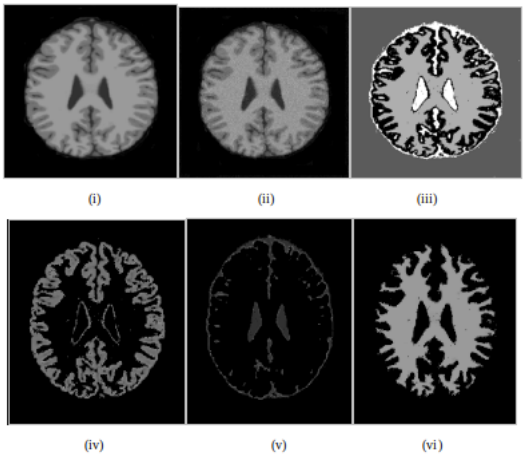

FIGURE 4. (i) MRI T1-99, (ii) MRI with 5% noise, (iii) MRI segmented using ACO-FCM, (iv) MRI with Gray, (v) CSF, (vi) MRI with White

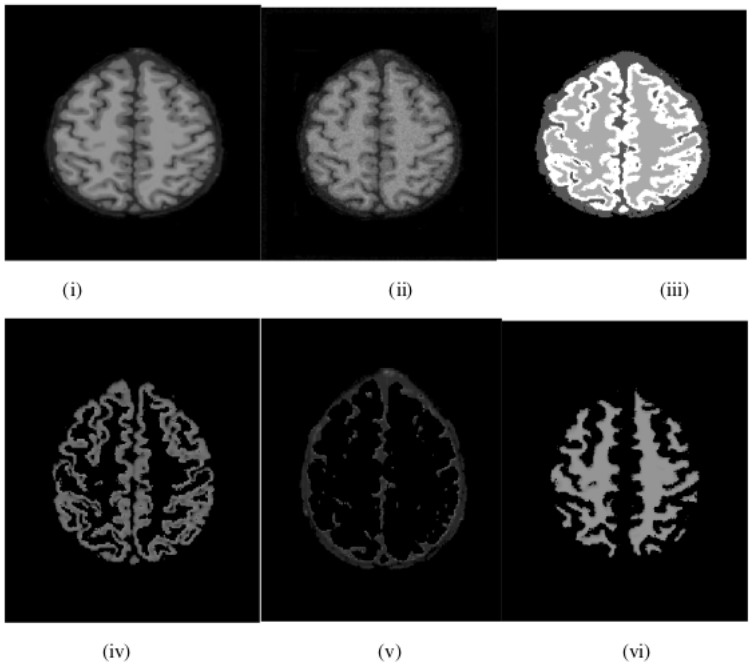

FIGURE 5. (i) MRI T1-126, (ii) MRI with 5% noise, (iii) MRI segmented using ACO-FCM, (iv) MRI with Gray, (v) CSF, (vi) MRI with White

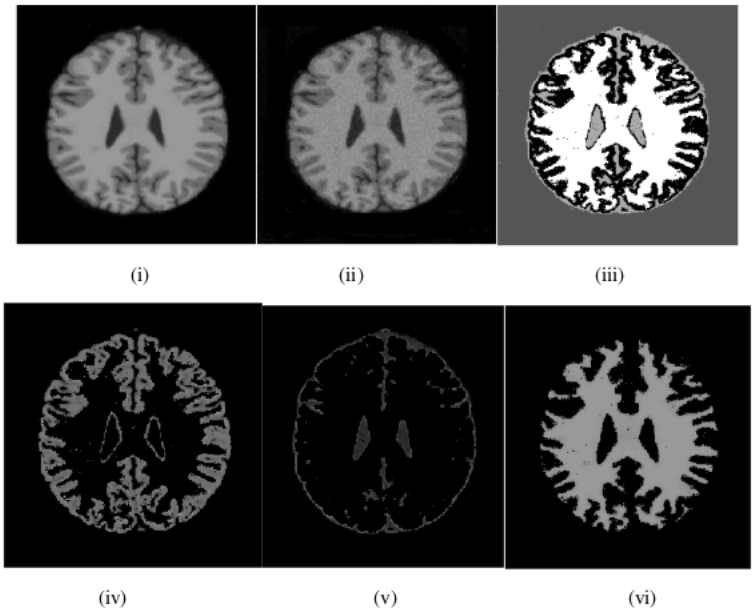

FIGURE 6. (i) MRI T1-100, (ii) MRI with 5% noise, (iii) MRI segmented using ACO-FCM, (iv) MRI with Gray, (v) CSF, (vi) MRI with White

10. CONCLUSION

You can find the global optimal solution with Ant Colony Optimization without being sucked into the local optimal solution. Significant improvement can be noticed in segmented images using ACO-based rather than random initialization. A noise reduction can be observed, as well as improved segmentation quality. As a solution to the problem of segmenting brain tissues, Ant Colony Optimization is proposed. Brain MRI images are segmented using ACO to determine initial cluster values. ACO-FCM outperforms standard FCM at both noise levels compared to standard FCM. As noise levels increase, FCM's efficiency decreases. Neither 3% nor 5% noise corrupts a slice. The accuracy of FCM decreases significantly at high noise levels, whereas the accuracy of ACO-FCM increases.

FUNDING

None

ACKNOWLEDGEMENT

None

CONFLICTS OF INTEREST

The author declares no conflict of interest.

REFERENCES

[1] S. Bricq, C. Collet, and J. P. Armspach, "Unifying framework for multimodal brain MRI segmentation based on Hidden Markov Chains," *Medical Image Analysis*, vol. 12, no. 6, pp. 639–652, 2008.
[2] B. Caldairou, N. Passat, P. A. Habas, C. Studholme, and F. Rousseau, "A non-local fuzzy segmentation method: Application to brain MRI," *Pattern Recognition*, vol. 44, no. 9, pp. 1916–1927, 2011.
[3] A. Mayer and H. Greenspan, "An adaptive mean-shift framework for MRI brain segmentation," *IEEE Transactions on Medical Imaging*, vol. 28, no. 8, pp. 1238–1250, 2009.
[4] Z. Ji, Y. Xia, Q. Sun, Q. Chen, D. Xia, and D. D. Feng, "Fuzzy local Gaussian mixture model for brain MR image segmentation," *IEEE Transactions on Information Technology in Biomedicine*, vol. 16, no. 3, pp. 339–347, 2012.
[5] B. Bhola, R. Kumar, P. Rani, R. Sharma, M. A. Mohammed, K. Yadav, S. D. Alotaibi, and L. M. Alkwai, "Quality-enabled decentralized dynamic IoT platform with scalable resources integration," *IET Communications*, 2022.
[6] P. Rani, S. Verma, S. P. Yadav, B. K. Rai, M. S. Naruka, and D. Kumar, "Simulation of the Lightweight Blockchain Technique Based on Privacy

and Security for Healthcare Data for the Cloud System," *International Journal of E-Health and Medical Communications (IJEHMC)*, vol. 13, no. 4, pp. 1–15, 2022.

[7] N. Kumar, P. Rani, V. Kumar, P. K. Verma, and D. Koundal, "TEEECH: Three-Tier Extended Energy Efficient Clustering Hierarchy Protocol for Heterogeneous Wireless Sensor Network," *Expert Systems with Applications*, vol. 216, pp. 119448–119448, 2023.

[8] N. Kumar, P. Rani, V. Kumar, S. V. Athawale, and D. Koundal, "THWSN: Enhanced energy-efficient clustering approach for three-tier heterogeneous wireless sensor networks," *IEEE Sensors Journal*, vol. 22, no. 20, pp. 20053–20062, 2022.

[9] B. Biswal, P. K. Dash, and S. Mishra, "A hybrid ant colony optimization technique for power signal pattern classification," *Expert Systems with Applications*, vol. 38, no. 5, pp. 6368–6375, 2011.

[10] K. Selvanayaki and P. Kalugasalam, "Brain tumor segmentation using algorithmic and non algorithmic approach," *International Journal of Research in Commerce, IT and Management*, no. 2, 2012.

[11] A. Nakib, H. Oulhadj, and P. Siarry, "A thresholding method based on two-dimensional fractional differentiation," *Image and Vision Computing*, vol. 27, no. 9, pp. 1343–1357, 2009.

[12] J. C. Bezdek *Pattern recognition with fuzzy objective function algorithms*, 2013.

[13] S. P. Yadav, M. Jindal, P. Rani, V. H. C. D. Albuquerque, C. D. S. Nascimento, and M. Kumar *An improved deep learning-based optimal object detection system from images*, 2023.

[14] S. Chen and D. Zhang, "Robust image segmentation using FCM with spatial constraints based on new kernel-induced distance measure," *IEEE Transactions on Systems, Man, and Cybernetics*, vol. 34, no. 4, pp. 1907–1916, 2004.

[15] D. L. Pham, "Fuzzy clustering with spatial constraints," *Proceedings. International Conference on Image Processing*, vol. 2, 2002.

[16] M. N. Ahmed, S. M. Yamany, N. Mohamed, A. A. Farag, and T. Moriarty, "A modified fuzzy c-means algorithm for bias field estimation and segmentation of MRI data," *IEEE Transactions on Medical Imaging*, vol. 21, no. 3, pp. 193–199, 2002.

[17] R. Krishnapuram and J. Kim, "A note on the Gustafson-Kessel and adaptive fuzzy clustering algorithms," *IEEE Transactions on Fuzzy Systems*, vol. 7, no. 4, pp. 453–461, 1999.

[18] D. E. Gustafson and W. C. Kessel, "Fuzzy clustering with a fuzzy covariance matrix," *IEEE Conference on Decision and Control Including the 17th Symposium on Adaptive Processes*, pp. 761–766, 1978.

[19] T. A. Runkler, "Ant colony optimization of clustering models," *International Journal of Intelligent Systems*, vol. 20, no. 12, pp. 1233–1251, 2005.

[20] Y. Kao and K. Cheng *An ACO-based clustering algorithm. International Workshop on Ant Colony Optimization and Swarm Intelligence*, pp. 340–347, 2006.

[21] A. N. Benaichouche, H. Oulhadj, and P. Siarry, "Multiobjective improved spatial fuzzy c-means clustering for image segmentation combining Pareto-optimal clusters," *Journal of Heuristics*, vol. 22, pp. 383–404, 2016.

[22] K. Kasiri, K. Kazemi, M. J. Dehghani, and M. S. Helfroush, "A hybrid hierarchical approach for brain tissue segmentation by combining brain atlas and least square support vector machine," *Journal of Medical Signals and Sensors*, vol. 3, no. 4, pp. 232–232, 2013.

[23] K. Kazemi and N. Noorizadeh, "Quantitative comparison of SPM, FSL, and brainsuite for brain MR image segmentation," *Journal of Biomedical Physics & Engineering*, vol. 4, no. 1, pp. 13–13, 2014.

[24] Brainweb *Simulated Brain Database*, 2023.